Arch. Metall. Mater. **66** (2021), 1, 259-266

DOI: 10.24425/amm.2021.134783

OSMAN ARMAĞAN[1*], TALIP KIRINDI[2]

EFFECT OF MN AMOUNT ON PHASE TRANSFORMATIONS AND MAGNETIC PROPERTIES IN Fe-Mn-Mo-Si ALLOYS

In this study, microstructural and crystallographic properties of phase transformations occurring with thermal effect in Fe-XMn-Mo-Si (X = 15.14wt.% ve 18.45wt.%) alloys have been investigated. The effects of (wt.%) Mn rates in the alloy on the characteristics of phase transformations were investigated by using Scanning Electron Microscopy (SEM), Transmission Electron Microscopy (TEM) and X-Ray Diffraction (XRD). SEM and TEM investigations was observed that two different martensite (ε and α') structures were formed in austenite grain. In addition, in TEM observations, the interface regions were selected over the bright field image. Crystallographic orientation relationships were obtained by the analyses of electron diffraction patterns from the interface regions. $\gamma \rightarrow \alpha'$ type transformation was observed for α' particle formation, and orientation relationship was found as $(\bar{1}11)_\gamma$ // $(011)_{\alpha'}$, $[101]_\gamma$ // $[\bar{1}1\bar{1}]_{\alpha'}$ and, $\gamma \rightarrow \varepsilon$ type transformation was observed for ε martensite plate formation, and the orientation relationship was found as $(\bar{1}1\bar{1})_\gamma$ // $(000\bar{2})_\varepsilon$, $[\bar{1}\,\bar{1}\,0]_\gamma$ // $[\bar{2}110]_\varepsilon$. It was noticed that this orientation relationships were compatible with the literature (Kurdjumov-Sachs and Shoji-Nishiyama orientation relationship). Precipitation phase (carbide) formation was observed in microstructure analyses. The changes in the magnetic properties of the alloys having different rates of Mn as a consequence of thermal effect phase transformations was investigated by using Mössbauer Spectroscopy. The internal magnetic field, volume fractions (transformation rates), isomer shift values and magnetic characteristics of the main and product phases were revealed by Mössbauer Spectroscopy. In the Mössbauer Spectrum, it was noticed that ε-martensite and γ-austenite structures showed paramagnetic single-peak, and α'-martensite showed ferromagnetic six-peaks.

Keywords: Fe-Mn-Mo-Si alloys, heat treatment, martensitic transformation, crystalloraphic properties, Mössbauer Spectroscopy

1. Introduction

Due to the micro and macro changes in materials and their technological use, phase transformations have become a subject of great interest today [1]. Within the scope of materials science, the word "phase" is used to describe homogeneous structures, where physical and chemical properties do not change. In a continuous matter, the crystal properties and the arrangement of atoms that are homogeneous in its own structure and as physically separated from the other parts of matter each region is defined as "phase". The transition from one equilibrium structure formed by certain phases to another equilibrium structure formed by different phases can take place in the structure, which is known as phase transformation [2]. Phase transformations that occur without changing the neighborhood of atoms during the event are called diffusionless phase transformations [3]. During the phase transformation, the chemical composition of the transformed and non-transformed regions does not change, only the crystal structure changes [4].

Metal alloys undergo a number of processes (heating, cooling, deformation, etc.) before they are converted into useful forms. The structure of the material is changed depending on the process conditions applied. These changes in the structure affect the properties of the material [5]. Towards the end of the 19th century in the study of metal and metal alloys, A. Martens first discovered the diffusionless phase transformation in metal and metal alloys [2,6]. Martensitic phase transformation occurs in all metals and metal alloys by cooling (or heating) the atoms so quickly that they cannot be displaced with by diffusion [7]. Firstly, martensite phase transformations in iron and iron based alloys have been observed as a result of the studies in many metals and metal alloys. The martensitic transformations in Fe-based alloys show crystallographically different transformations. These occur as the transformation of the main phase in the face-centered

[1] KARAMANOĞLU MEHMETBEY UNIVERSITY, DEPARTMENT OF MEDICAL SERVICES AND TECHNIQUES, VOCATIONAL SCHOOL OF HEALTH SERVICE, PROGRAM OF OPTICIANRY, 70200, KARAMAN, TURKEY
[2] KIRIKKALE UNIVERSITY, FACULTY OF EDUCATION, DEPARTMENT OF MATHEMATIC AND SCIENCE EDUCATION, YAHSIHAN 71450, KIRIKKALE, TURKEY

* Corresponding author: o_armagan@windowslive.com

© 2020. The Author(s). This is an open-access article distributed under the terms of the Creative Commons Attribution-NonCommercial License (CC BY-NC 4.0, https://creativecommons.org/licenses/by-nc/4.0/deed.en which permits the use, redistribution of the material in any medium or format, transforming and building upon the material, provided that the article is properly cited, the use is noncommercial, and no modifications or adaptations are made.

cubic (f.c.c.) structure to the martensite phase in body-centered cubic (b.c.c.), body-centered tetragonal (b.c.t.) or close-packed hexagonal (h.c.p.) structures [6,8-11]. Today, metal and metal alloys occupy a very important place commercially. In particular, Fe-based alloys exhibit good mechanical properties and shape memory effect thanks to their martensitic phase transformations. In addition, the investigation of Fe-Mn and Fe-Mn based alloys among Fe-based alloys has become widespread [12-14]. Jun and Choi studied the effects of Mn amount on microstructure in Fe-Mn alloys [12]. In Fe-Mn alloys, two kinds of martensite may occur depending on the amount of Mn in the alloy. These are ε and α' martensities. Percentage (wt.%) of Mn amount is effective in this formation. If the Mn volume in the alloy is less than 10 percent (wt.%), α' martensite is observed intensively. If the Mn content of the alloy is more than 15 percent (wt.%), ε martensite formation is observed intensively. Both types of martensite species have different transformation properties and different physical properties [6,15,16].

With the addition of other alloying elements (such as Mo, Si, Co) to Fe-Mn based alloys, many physical properties of the material (such as transformation rate, transformation amount, mechanical properties) can be improved. For example, the addition of Si increases the shape-memory effect of the alloy [17]. On the other hand, Mo can be added to increase the strength and hardness of the alloy [13]. For these reasons, Fe-Mn-X type alloys have received considerable attention. Marinelli et al studied the austenite-martensite type phase transformations in Fe-Mn-Co alloy [18].

Mössbauer Spectroscopy method is very important for the determination of magnetic properties. Mössbauer Spectroscopy has been widely used in alloy physics because it is a suitable technique for characterizing the configuration of atoms in solids of crystals [19,20]. In addition, Mossbauer spectroscopy is a technique mainly used as transmission and is very suitable not only for crystalline materials but also for amorphous materials [67-69]. In the case of Fe-based alloys, extensive research has been carried out since 1960 on martensite [21] and retained austenite [22,23] phases, by using Mössbauer Spectroscopy [24]. In previous studies: It has been shown by using Mössbauer Spectroscopy method that internal magnetic field decreases with increasing Si amount in $Ni_3Fe_{1-x}Si_x$ alloy [25]. In the studies performed on Fe-33%Ni-0.7%C alloy and Fe-Ni-C alloys, it was shown by using Mössbauer Spectroscopy method that the internal magnetic field of the alloy decreased as the heat treatment temperature increased [26,27]. In a study carried out by Armağan et al., ε martensite and α' martensite structure formations obtained by adding Mo and Co to Fe-Mn based alloys were observed and by using Mössbauer Spectroscopy were investigated volume quantities and crystallography of these martensites [28]. XRD and Mössbauer Spectroscopy have been extensively used to determine the relative fraction of ε type martesite occurring in Fe-Mn based alloys [15]. In an earlier study, for Fe-Mn alloys, Acet et al. investigated the magnetic properties of $\gamma \rightarrow \varepsilon$ and $\gamma \rightarrow \alpha'$ austenite-martensite type transformations [16]. In Fe based alloys, generally austenite phase and ε martensite phase paramagnetic and α' martensite phase show a ferromagnetic property. In Fe based alloys, generally austenite phase and ε martensite phase paramagnetic and α' martensite phase show a ferromagnetic property [29-32]. In this study, the effect of Mn amount on martensitic transformations in Fe-Mn-Mo-Si alloys containing different amounts of Mn is discussed. SEM, TEM, X-Ray and Mössbauer Spectroscopy methods were used to search the morphological, crystallographic and magnetic characters of the alloys.

2. Experimental

The alloys used in the experiments were obtained by melting (99.9%) pure elements (Fe, Mn, Mo, Si) in argon atmosphere and quenching them as cylindrical rods. These cylindrical rods are 10 cm long and 1 cm in diameter (Ingot). Alloys were prepared by using the arc melting technique. Two alloys consisting of these elements were prepared: Fe-15.14% Mn-5.10% Mo-2.18% Si and Fe-18.45% Mn-4.69% Mo-1.99% Si (Table 1). These chemical rates were determined using Electron Dispersion Spectroscopy (EDS). The ingot-shaped alloys were cut into 1 (or 2) cm length pieces with a diamond cutter at room temperature, and the cutting samples were sealed into quartz capsules by vacuuming. These samples were placed in quartz tubes and put into a heat treatment furnace. The heat treatments applied were given in Table 2. Sanding (sandpapers) and polishing were applied to the surfaces of the samples for SEM examinations. The samples were left in a solution consisting of 5% nitric acid and 95% methanol (throughout 30 seconds) to finally correct the sample surfaces. The JEOL 5600 device was used for SEM observations (20 kV). EDS analyzes were performed while micro photographs were taken from samples prepared for SEM studys.

TABLE 1

Chemical composition of the studied alloys (wt.%)

Alloys (wt.%)	Chemical compositions (wt.%)				
	Fe	Mn	Mo	Si	C
Fe-15.14 Mn-5.10 Mo-2.18 Si **(A)**	77.17	15.14	5.10	2.18	0.015
Fe-18.45 Mn-4.69 Mo-1.99 Si **(B)**	74.43	18.45	4.69	1.99	0.048

TABLE 2

Heat treatments of alloys

Samples	Nature of heat treatments
A	Homogenized at 1200°C for 2 h and quenched in water bath at room temperature
B	Homogenized at 1200°C for 2 h and quenched in water bath at room temperature

Samples of 40-60 μm thick and 3 mm diameter were prepared for TEM observations. First the samples were cut by a diamond cutter and then thinned by sandpaper. In the next

stage, a solution was prepared for the samples. This solution was created from a mixture of 90% acetic acid and 10% perchloric acid. With this solution, double jet electro-polishing (drilling) were applied in the Streurs-tenupol Jet unit at a temperature of between –15°C to 10°C and with a voltage of 20V. For TEM investigations, a JEOL 3010 device was used operating at 300 kV.

Volume fractions of α' and ε phases were measured by XRD method. The Rigaku Geigerflex D-MaxB X-Ray diffractometer was used as the XRD device (Cu Kα radiation and monochromatic from an angle of 20-80° (2θ) with a step size of 0.02° 2θ and a counting time of 6 s step^{-1}). In a previous study, lattice constants were calculated using the following formula:

$$a_\gamma = \frac{\sqrt{h^2k^2l^2}}{2\sin\theta_{hkl}}$$

where λ, (hkl), and θ_{hkl} are the wavelength of the radiation, the three Miller indices of a plane and the Bragg angle, respectively [33,34].

Mössbauer Spectroscopy was used to study the magnetic characters of main and product phases. The samples were prepared in the form of discs 40-60 μm thick and 3 mm in diameter. Measurements were made at room temperature. The radioactive source of the spectrometer used is 50 mCi ^{57}Co. A Normos-90 computer program was used to obtain Mössbauer parameters. The Mössbauer spectra of the examined sample were calibrated α-Fe, and isomer shifts were given relative to the center of the α-Fe.

3. Results and discussion

3.1. Microstructure investigations

The sample (sample A) in Fe-15.14% Mn-5.10% Mo-2.18% Si alloy was subjected to heat treatment at 1200°C for 2 hours and cooled rapidly in water at room temperature. The SEM image of this sample is given in Figure 1a,b. SEM images showed that the structure remained in the austenite phase and the austenite grains were clearly seen. These grain sizes are known to vary depending on the heat treatment temperature, duration and cooling method. In general, it was observed that grain size increased with increasing heat treatment temperature and time in iron and iron alloys [35,36]. As reported in the literature, identical atom arrays at grain boundaries cannot be mentioned because they contain defects such as dislocations, interatomic spacing and impurity atoms [6]. Also, the precipitates were formed besides the austenite phase. In the SEM image taken at high magnification in Figure 1b, the carbide precipitates formed at the grain boundary were clearly observed. On the other hand, small amount of carbide precipitates were observed with in grain areas. In a study by Wang Bin, the iron-carbide morphology of hypereutectic steels was investigated and as shown in the our SEM image, the presence of precipitates along the grain boundaries is observed [37].

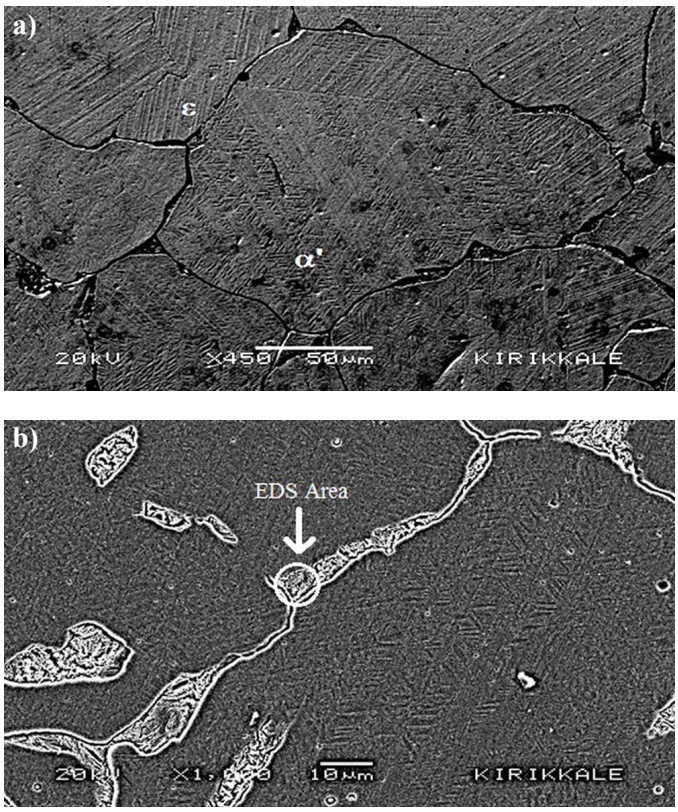

Fig. 1. SEM micrographs showing the microstructure of A sample a) α' and ε martensite b) Precipitate (EDS)

ε martensite plates and α' particles were found in the surface investigations of structure. Here, it was observed that ε martensite plates were formed in a stacked way as parallel to each other, whereas α' particles were formed as small complex structures. The effects of grain boundaries on martensite plate formations are described in a study conducted by Easterling and Porter [38]. It was found that grain boundaries prevented the growth of martensite plates and the martensite nucleation numbers had no effect on the grain size, but the shape and size of the formed martensite plates were a function of the grain size [39-43].

EDS results for sample A are given in Table 3. According to the results of EDS analysis, Mo element showed a very high increase. As it is known, Mo is a carbide-forming element. The increase in Si along with Mo is remarkable. These two elements have replaced Fe and Mn at the grain boundaries. This formation, known as the precipitate phase, is a condition that occurs generally at the grain boundaries. As a result of homogenisation and rapid cooling in water, the accumulation and precipitation of Mo and Si at the grain boundaries (ie in the precipitate area) has produced a significant result. It is stated that the formation of precipitation at the grain boundary is a thermodynamic result in alloys [44]. According to the literature, it is known that the precipitations at the grain boundaries increase the strength and hardness by preventing the transformation, increase the resistance of the material against cohesions by increasing the ductility and toughness and produce different morpholological results for superalloys [45,46].

TABLE 3

EDS analysis datas

Elements	Fe (wt.%)	Mn (wt.%)	Mo (wt.%)	Si (wt.%)	C (wt.%)	Total (wt.%)
1. Area	69.29	14.08	11.60	4.67	0.36	100

The SEM image of the B sample, which was heat treated at 1200°C for 2 hours and cooled rapidly in water at room temperature, is given in Figure 2a,b. The surface examination of the alloy showed that most of the structure remained in the austenite phase and grains were formed in the sample. It was observed that the grains formed belong to austenite phase with a size of 50-200 µm. The shape and size of these grains is in accordance with the literature [6,47]. According to the first sample in Fe-15.14%Mn-5.10%Mo-2.18%Si alloy homogenized at the same temperature, austenite grains became larger and more prominent in addition to the increase of Mn rate [5].

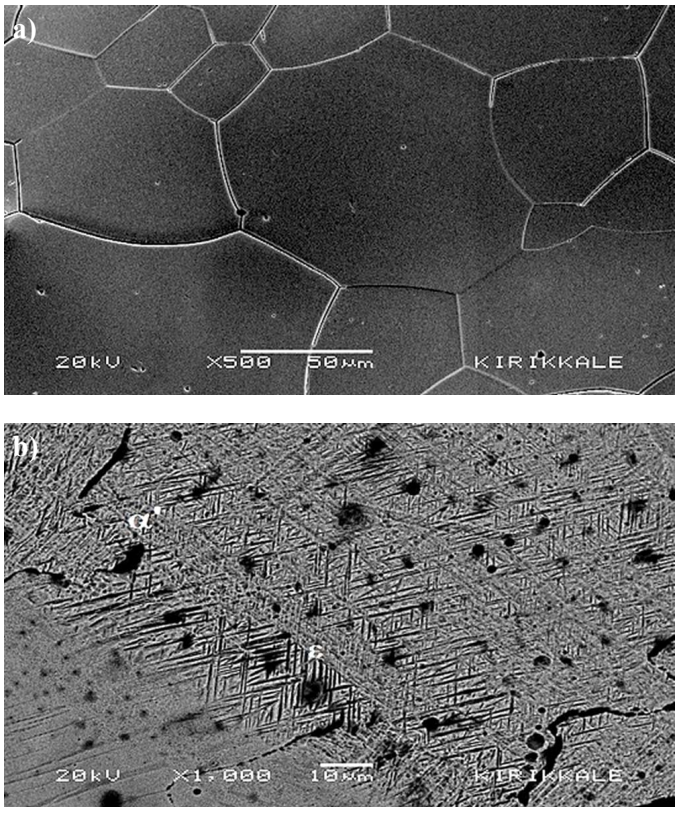

Fig. 2. SEM micrographs showing the microstructure of B sample a) Austenite grains b) α' and ε martensite

In addition, two different structures were observed in some areas within austenite grain. These are ε martensite plates stacked in parallel with each other and α' particles formed in the form of lenticular size complex structures (Fig. 2b). Here, the driving force required for the formation of the martensitic transformation was obtained with the temperature difference resulting from rapid cooling [4,47]. α' martensite formation was quite decreased compared to sample A while ε martensite amount increased.

3.2. TEM investigations

The sample in Fe-15.14%Mn-5.10%Mo-2.18%Si alloy was annealed at 1200°C. TEM image of the sample, and electron diffraction patterns with index diagrams are given in Figure 3. Both ε martensite structure and α' martensite structure were observed in the images taken from selected regions. In the electron diffraction pattern in Figure 3 (diffraction pattern in the upper left corner), the orientation relationship for $\gamma \rightarrow \alpha'$ type martensite transformation was found as $(\bar{1}11)_\gamma$ // $(011)_{\alpha'}$, $[101]_\gamma$ // $[\bar{1}1\bar{1}]_{\alpha'}$. It was observed that this orientation relationship was consistent with the literature [6]. By measuring the distances "d" between the reflecting planes, lattice constants were calculated as $a_\gamma \cong 3{,}5989$ Å for f.c.c. structure and $a_{\alpha'} \cong 2{,}8567$ Å for b.c.c. structure. In the other electron diffraction pattern in Figure 3 (diffraction pattern in the lower left corner), the orientation relationship for $\gamma \rightarrow \varepsilon$ type martensite transformation was found as $(\bar{1}1\bar{1})_\gamma$ // $(000\bar{2})_\varepsilon$, $[\bar{1}\,\bar{1}\,0]_\gamma$ // $[\bar{2}110]_\varepsilon$. It was observed that this

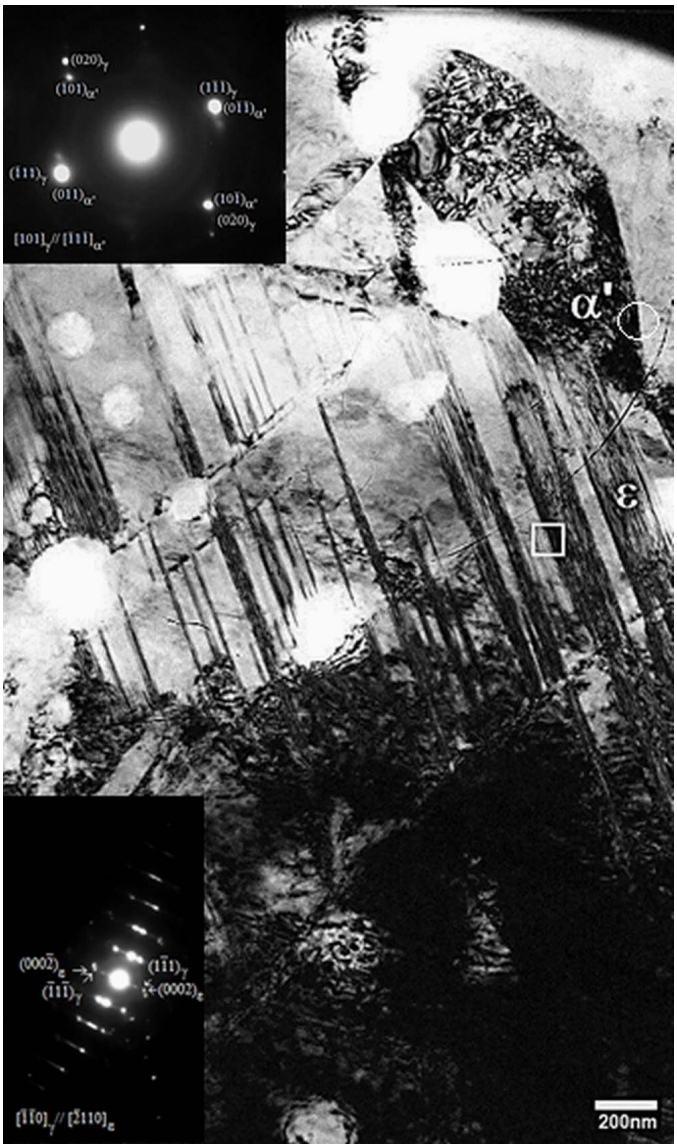

Fig. 3. Bright field TEM image and electron diffraction patterns obtained from the selected areas (interfaces) for sample A

orientation relationship was in accordance with the literature [6]. By measuring the distances "d" between the reflecting planes, lattice parametres were calculated as $a_\gamma \cong 3{,}5967$ Å for f.c.c. structure and $a_\varepsilon \cong 2{,}5615$ Å, $c_\varepsilon \cong 4{,}0229$ Å for h.c.p. structure.

In Figure 3, ε martensite was observed in the form of parallel plates. It can be said that the stacking faults required for ε martensite plate formation are increased for this sample and these defects combine to form ε martensite plates [48-50]. It is thought that the ε plates in Figure 3 may be formed by the combination of many stacking faults or by the effect of other defects in the austenite phase [6]. The embryo required for the formation of ε martensite occurs due to stacking faults in the austenite phase. Approaches that explain this situation are based on the hypothesis that the stacking faults overlap every second close-plane of the austenite structure and the conversion occur with the displacement of Shockley partial dislocations $a_{\text{f.c.c.}}/6\langle 112\rangle$ [13,51-53]. a¢ martensite particles, another type of martensite in the TEM image, was observed to form as small complex structures and this formation was thought to be related to dislocations in the previous austenite phase. Therefore, dislocations occur in areas of austenite are seen [6,54]. ε and α' martensites formed by cooling of the heat treated alloy was revealed by TEM images. This result is consistent with current SEM observations. In general, in Fe-Mn based alloys, researches on martensitic phase transformation have shown that γ structure can be converted to ε and α' structures and $\varepsilon \rightarrow \alpha'$ conversion is possible under certain physical conditions [55].

TEM image of sample B annealed at 1200°C is given in Figure 4. ε martensite plates and precipitate phase formation was observed in this sample. Electron diffraction image taken from the precipitate phase region was given in Figure 4 (upper right corner). According to the sample in Fe-15.14%Mn-5.10%Mo-2.18%Si alloy annealed same heat treatment temperature, it was observed that ε martensite plates were formed in a thicker way (Fig. 4).

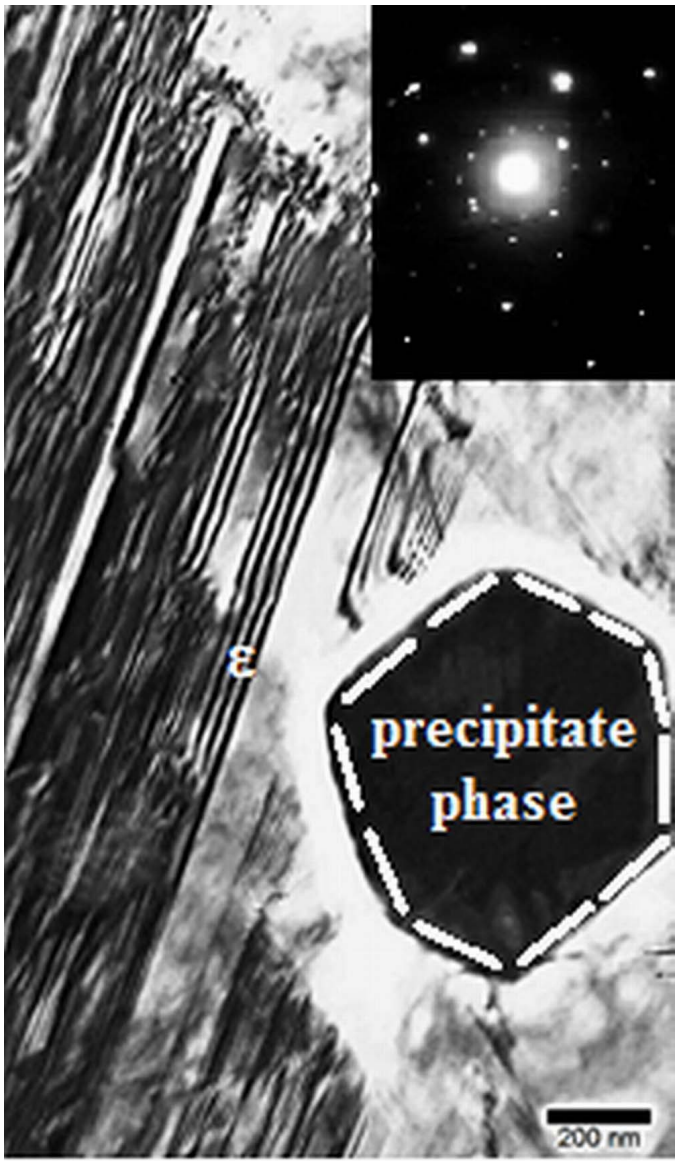

Fig. 4. Bright field TEM image and electron diffraction patterns obtained from the selected area (precipitate phase) for sample B

3.3. XRD analyses

XRD measurements of sample A homogenized at 1200°C are given in Figure 5a. In the XRD investigations, the peaks belonging to diffraction giving planes of this sample were obtained for the austenite structure $(111)_\gamma$, $(200)_\gamma$, $(220)_\gamma$, for the α' martensite structure $(110)_{\alpha'}$, $(200)_{\alpha'}$ and for the ε martensite structure $(002)_\varepsilon$, $(101)_\varepsilon$, $(110)_\varepsilon$. Lattice parameters calculated from the peaks obtained according to XRD measurements for this sample: were calculated as $a_\gamma \cong 3{,}6194$ Å for the (200) plane of f.c.c. structure, $a_{\alpha'} \cong 2{,}8842$ Å for the (110) plane of b.c.c. structure, $a_\varepsilon \cong 2{,}5722$ Å, $c_\varepsilon \cong 4{,}0687$ Å for the (002) plane of h.c.p. structure (Table 4).

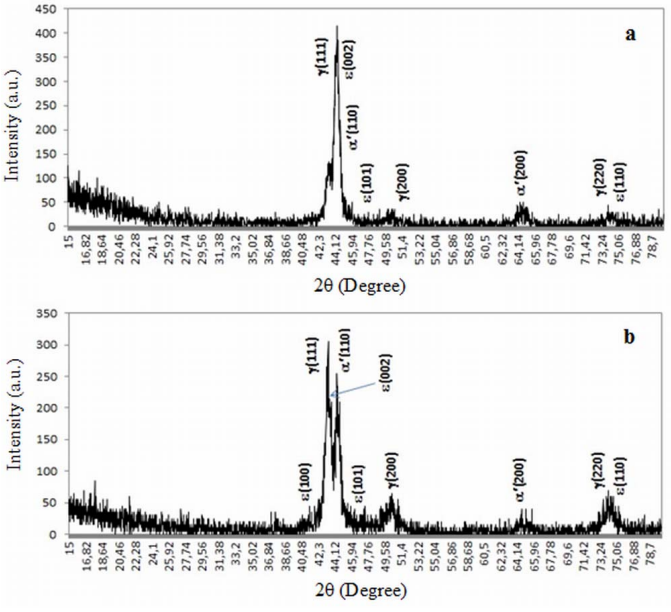

Fig. 5. XRD measurements of belonging to samples of homogenized at 1200°C for 2 h and quenched in water bath at room temperature a) A sample b) B sample

TABLE 4

The lattice parameter of γ, ε and α' phases in A and B alloys

Alloys	Lattice parameters (A°)			
	γ phase	α' phase	ε phase	
	(a_γ)	($a_{\alpha'}$)	(a_ε)	(c_ε)
A	3.6194	2.8842	2.5722	4.0687
B	3.6156	2.8854	2.5823	4.4031

XRD measurements of sample B are given in Figure 5b. In this sample, the peaks belonging to diffraction giving planes $(111)_\gamma$, $(200)_\gamma$, $(220)_\gamma$ of austenite phase were observed. At the same time, the peaks belonging to diffraction giving planes $(110)_{\alpha'}$, $(200)_{\alpha'}$ of b.c.c. structure were obtained and the peaks belonging to diffraction giving planes $(100)_\varepsilon$, $(101)_\varepsilon$, $(002)_\varepsilon$ and $(110)_\varepsilon$ of h.c.p. phase. Lattice parameters calculated from the peaks obtained according to XRD measurements for this sample; were calculated as $a_\gamma \cong 3{,}6156$ Å for the (200) plane of f.c.c. structure, $a_{\alpha'} \cong 2{,}8854$ Å for the (110) plane of b.c.c. structure, $a_\varepsilon \cong 2{,}5823$ Å, $c_\varepsilon \cong 4{,}4031$ Å for the (100) plane of h.c.p. structure (Table 4).

As understood from the peaks in the XRD graphs given in Figure 5a,b: ε martensite formation is more intense in B sample compared to A, while α' martensite formation is more intense in A sample compared to B. On the other hand, when the volume quantities remaining as austenite phase for both samples are compared, the volume amount of austenite in sample B is greater than that of A.

3.4. Mössbauer spectroscopy analyses

Through Mössbauer Spectroscopy, the magnetic states of the main phase and product phases, conversion percentages, isomer shift values, and the internal magnetic fields of the product phases can be determined [6]. The Mössbauer effect arises from transitions between energy levels in atomic nucleus as a result of absorption of γ rays by the material [6]. In Fe-Mn alloys, the γ and ε phases usually show paramagnetic properties, while the α' phase exhibits ferromagnetic properties [55-57]. Samples exhibiting paramagnetic properties in the Mössbauer Spectrometer give single peaks, while samples exhibiting ferromagnetic and antiferromagnetic properties give sextet peaks [29,31].

According to the data obtained from the Mössbauer Spectroscopy of the A and B samples which were heat treated at different temperatures and cooled rapidly in the water at room temperature, the single paramagnetic peak of the ε martensite and γ austenite structures and the six ferromagnetic peaks of the α' martensite were observed (Fig. 6a,b). When we look at the transformation percentages of the product phase (α' martensite) showing ferromagnetic properties, a higher amount of formation was observed in the A sample (Table 5). Reason of this may be due to the fact that at higher Mn rates, the structure is more prone to remain in the austenite phase and therefore the product phase formation occurs in smaller amounts. The volume quantities (transformation percentages) of austenite and martensite phases formed in an alloy can be determined by Mössbauer Spectroscopy method. These transformation percentages are calculated thanks to the different magnetic characteristics showed of the phases. However, in this study, since both γ austenite and ε martensite phases show paramagnetic properties, it is not possible to differentiate these phases by Mössbauer Spectroscopy at room temperature [55].

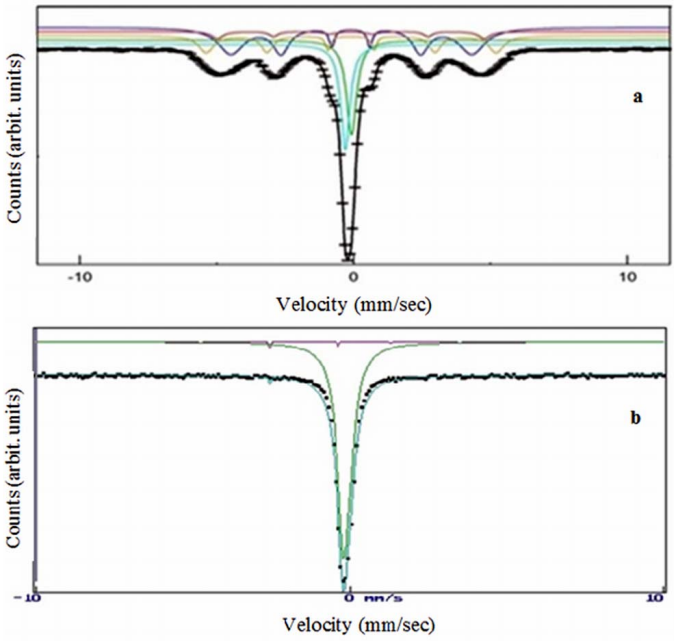

Fig. 6. Room temperature Mössbauer spectra of a) A sample b) B sample

TABLE 5

Mössbauer Spectroscopy values in the thermally induced alloys

Samples	$\gamma + \varepsilon$ phase (%)	α' phase (%)	$\delta_{\gamma+\varepsilon}$ (mm/s)	$\delta_{\alpha'}$ (mm/s)	B_{hf} (Tesla) (α')
A	48.266	51.734	–0.2012	0.0083	32.7510
B	97.600	2.400	–0.1597	0.2675	31.7586

α' martensite formation was quite intense in A sample (15 wt.% Mn), while decreased significantly in B sample (18 wt.% Mn) (Table 5). Based on this result, it can be said that 15 wt.% Mn rate is very suitable for α' martensite formation. When the product phases formed after heat treatment in samples A and B were taken into consideration, it was found that sample B with a high Mn content had a lower internal magnetic field value than sample A with a low Mn content (Table 5).

Foreign substances such as Si, Mn, Mo, Cr and Cu may reduce the magnetic field of Fe atoms [24]. The magnetic properties of Fe-Mn based alloys change according to the Mn amount. As the Mn amount increases, the internal magnetic field decreases, which means that as the Mn amount increases, the ferromagnetic character decreases and at high Mn values it can disappear completely [58]. In previous studies of Fe-based alloys have been reported that the internal magnetic field decreases in alloys with Mo or Si additions. [59]. In addition, the reduce in

the internal magnetic field indicates a reduce in the magnetic moment, this can be attributed to an increase in electron transfer for unfilled 3d bands [60,61]. Because in the 3d shell of the Fe atom, there are only single electron in 4 energy levels. They rotate in the same direction and their magnetic poles are parallel to each other. This electron structure explains why Fe has a high magnetism. The reduce of the internal magnetic field shows that the magnetic moment of iron is decreased by the increase of electron transfer to the 3d shell [62].

When isomer shift values belonging to austenite phases for both alloys were compared, the austenite phase belonging to sample A showed more isomer shift values (Table 5). It is possible to say that the differences in isomer shift values are because of concentration changing in the s-electron bands of the alloying elements. By the electron density in the 3d band of Fe increases, the electron density in the 3s and 4s band decreases, so the isomer shift values increase [63,64].

In Fe-Mn based alloys containing Co, austenite lattice constants have been observed to increase by the increase of Mn content. On the other hand, elements such as Cr, Al, and Si added to Fe-Mn-based alloys have been reported to affect austenite lattice parameters [65]. This effect is relating with the atomic radius of the elements that make up compounds of Fe in Fe-Mn alloys. These alloy atoms are larger than the Fe atom and for this reason increase the lattice constants. To support this situation, the atomic radius of Mn (0.127 nm) is also greater than the radius of Fe (0.126 nm) and causes the lattice parameter to increase in Fe-Mn-Co alloys [58]. Also in a study by Jung et al. on the Mn effect, isomer shift (relative to α'-Fe) and internal magnetic field values were said to decrease with the number of nearest neighbor Mn atoms [66].

4. Conclusions

In this study, the effects of phase transformations occurring with thermal effect in Fe-X(wt.%)Mn-Mo-Si (X =1 5.14% ve 18.45%) alloys with different Mn rates were investigated on microstructure, crystallographic properties and magnetic properties.

- In the SEM studies of A and B samples, which were subjected to heat treatment for 2 hours at 1200°C and cooled rapidly by throwing into water at room temperature, the formation of ε and α' martensite structures together with austenite phase were observed. It was understood that austenite lattice parameters increased in both alloys containing high Mn rate. In sample B, with increasing Mn rate (according to sample A) austenite grains were observed to become larger and more pronounced. Again in sample B (according to the sample A) amount of α' martensite is significantly reduced while increasing the amount of ε martensite was observed. In addition, precipitate phase (carbide) formation was observed in SEM investigations of sample A.
- According to the analyses of electron diffraction patterns taken from the interfaces at TEM examinations of A sample: Martensitic transformations of type $\gamma \rightarrow \alpha'$ and $\gamma \rightarrow \varepsilon$ were observed. Crystallographic orientation relationships:

  $(\bar{1}11)_\gamma$ // $(011)_{\alpha'}$, $[101]_\gamma$ // $[\bar{1}1\bar{1}]_{\alpha'}$

  $(\bar{1}1\bar{1})_\gamma$ // $(000\bar{2})_\varepsilon$, $[\bar{1}\,\bar{1}\,0]_\gamma$ // $[\bar{2}110]_\varepsilon$ was obtained as.

  At the same time, according to electron diffraction pattern analyses, it was understood that α' martensite crystallized in b.c.c. structure and ε martesite crystallized in h.c.p. structure. On the other hand, the TEM investigations of the B sample was observed precipitate phase formation with ε martensite.
- Lattice parameters belong to martensite structures observed in SEM and TEM studies were calculated from XRD analysis datas.
- In Mössbauer Spectroscopy that was determined that the γ and ε phases showed paramagnetic properties and the α' phase showed ferromagnetic properties. Table 5 was created according to Mössbauer Spectroscopy analysis datas. In this way, data such as internal magnetic field, isomer shift and formation quantities were compared for A and B samples. In sample A, an internal magnetic field of 32.7510 T was measured and it was observed that the amount of α' martensite was quite high. In sample B, the internal magnetic field value of 31.7586 T was measured and the amount of α' martensite was found very low.

Acknowledgements

This study was supported by Kırıkkale University Scientific Research Fund with Project number 2016/131.

REFERENCES

[1] P. Chowdhury, D. Canadinc, H. Sehitoglu, Mater. Sci. Eng. R **122**, 1-28 (2017).
[2] T.N. Durlu, F.Ü. Fen ve Müh. Bilimleri Dergisi **13** (1), 1-11 (2001).
[3] J.W. Christian, The Theory of Transformation in Metals and Alloys, Pergamon Press, London (1975).
[4] L. Kaufman, M. Cohen, Progress in Metal Physics **7**, 165-246 (1958).
[5] D.R. Askeland, The Science and Engineering of Materials, Chapman and Hall, London (1990).
[6] Z. Nishiyama, Martensitic Transformations, Academic Press., New York (1978).
[7] M. Cohen, G.B. Olson, P.C. Clapp, In Proc. Intl. Conf. Mart. Trans. ICOMAT-79, Cambridge, MA, M.I.T, 1 (1979).
[8] S. Kajiwara, Mater. Sci. Eng. A **273-275**, 67-88 (1999).
[9] G.B. Olson, M. Cohen, Metall. Trans. A **7** (12), 1897-1904 (1976).
[10] G.B. Olson, M. Cohen, Metall. Trans. A **7** (12), 1905-1914 (1976).
[11] G.B. Olson, M. Cohen, Metall. Trans. A **7** (12), 1915-1923 (1976).
[12] J.H. Jun, C.S. Choi, Mater. Sci. Eng. A **252**, 133 (1998).
[13] T.N. Durlu, J. Mater. Sci. Lett. **16**, 320-321 (1997).
[14] T. Kirindi, E. Güler, M. Dikici, J. Alloys Compd. **433**, 202 (2007).

[15] J. Martínez, S.M. Cotes, A.F. Cabrera, J. Desimoni, A. Fernández Guillermet, Mater. Sci. Eng. A **408**, 26 (2005).
[16] M. Acet, T. Schneider, B. Gehrmann, E.F. Wassermann, J. Phys. IV **5**, 379 (1995).
[17] S. Cotes, A. Fernández Guillermet, M. Sade, J. Alloys Compd. **278**, 231 (1998).
[18] P. Marinelli, A. Baruj, S. Cotes, A. Fernández Guillermet, M. Sade, Mater. Sci. Eng. A **273-275**, 498 (1999).
[19] U. Gonser (Ed.), Mössbauer Spectroscopy, Topics in Applied Physics Series: Vol. 5, Springer-Verlag, Berlin (1975).
[20] S. Kobayashi, K. Asayama, J. Itoh, J. Phys. Soc. Jpn. **21** (1), 65 (1966).
[21] H. Ino, T. Ito, S. Nasu, U. Gonser, Acta Metall. **30**, 9 (1982).
[22] M.C. Cadeville, J.M. Friedt, C. Lerner, J. Phys, F Met. Phys. **7** (1), 123 (1977).
[23] A. Mijovilovich, A. Goncalves Vieira, R. Paniago, H.D. Pfannes, B.Mendonc Gonzalez, Mater. Sci. Eng. A **283**, 65 (2000).
[24] M. Liu, P. Liu, B. Shib, X. Cai, H. Song, Materials Chemistry and Physics **99**, 183-189 (2006).
[25] T.V.S.M. Mohan Babu, C. Bansal, J. Mater. Sci. Lett. **32**, 1587 (1997).
[26] F.Z. Bentayeb, B. Bouzabata, S. Alleg, Hyperfine Int. **128**, 375 (2000).
[27] K.G. Binnatov, A.O. Mekhrabov, Turkish Journal of Physics. **25**, 121 (2001).
[28] O. Armağan, U. Sarı, Ç. Yücel, T. Kırındı, Micron **103**, 34-44 (2017).
[29] J.H. Yang, H. Chen, C.M. Wayman, Metall. Trans. A **23**, 1439 (1992).
[30] M. Mizrahi, A.F. Cabrera, S.M. Cotes et al., Hyperfine Interact. **156/157**, 541 (2004).
[31] S.M. Cotes, A.F. Cabrera, L.C. Damonte et al., Hyperfine Interact. **141/142**, 409 (2002).
[32] İ. Akgün, A. Gedikoglu, T.N. Durlu, J. Mater. Sci. **17**, 3479-3483 (1982).
[33] X. Tan, Y. Xu, X. Yang, Z. Liu, D. Wu, Mater. Sci. Eng. A **594**, 149-160 (2014).
[34] X. Tan, Y. Xu, X. Yang, D. Wu, Mater. Sci. Eng. A **589**, 101-111 (2014).
[35] T. Shiming, L. Jinhai, Y. Shiwei, Scripta Metall. Mater. **25**, 2613 (1991).
[36] B.H. Jiang, L. Sun, R. Li, T.Y. Hsu, Scripta Metall. Mater. **33**, 63 (1995).
[37] W. Bin, L. Zhenyu, Z. Xiaoguang, W. Guodong, R.D.K. Misra, Mater. Sci. Eng. A **575**, 189-198 (2013).
[38] D.A. Porter, K.E. Easterling, Phase Transformations in Metals and Alloys, Chapman and Hall, London (1981).
[39] N. Bergeon, G. Guenin, C. Esnouf, Mater. Sci. Eng. A **242**, 87-95 (1998).
[40] G.J. Arruda, V.T.L. Buono, M.S. Andrade, Mater. Sci. Eng. A **273-275**, 528-532 (1999).
[41] B.J. Maji, M. Krishnan, Scripta Mater. **48**(1), 71-77 (2003).
[42] B.H. Jiang, L. Sun, R. Li, T.Y. Hsu, Scripta Metall. Mater. **33**, 63 (1995).
[43] Reyhani, M.M., Mc Cormick, P.G., Mater. Sci. Eng. A **160**, 57-61 (1993).
[44] T. Horıuchı, N. Satoh, Hokkaido Institute Of Technology, Japan,165-173 (2013).
[45] S. Ratanaphan S, Y. Yoon, G.S. Rohrer, J. Mater. Sci. **49** (14), 4938-4945 (2014).
[46] W. Chen, M.C. Chaturvedi, The Minerals, Metals & Materials Society, (1994), DOI: 10.7449/1994/Superalloys_1994_567_577.
[47] Y.T. Hsu, X. Zuyao, Mater. Sci. Eng. A **273-275**, 494-497 (1999).
[48] H. Inagaki, Z. Metallkd. **83**, 90-96 (1992).
[49] T. Aikawa, Y. Nishino, S. Asano, Scripta Metall. Mater. **29**, 135 (1993).
[50] S. Takaki, H. Nakatsu, Y. Tokunaga, Mater. Trans. JIM **34**, 489 (1993).
[51] T.N. Durlu, J. Mater. Sci. **34**, 2887-2890 (1999).
[52] T.N. Durlu, J. Mater. Sci. Lett. **15**, 2134-2136 (1996).
[53] T. Kırındı, M. Dikici, J. Alloys Compd. **407**, 157-162 (2006).
[54] E. Güler, T. Kırındı, H. Aktaş, J. Alloys Compd. **440**, 168-172 (2007).
[55] U. Sarı, T. Kırındı, M. Yüksel, S. Ağan, J. Alloys Compd. **476**, 160-163 (2009).
[56] U. Sarı, E. Güler, T. Kırındı, M. Dikici, J. Phys. and Chem. Solids **70**, 1226-1229 (2009).
[57] T. Kırındı, U. Sarı, J. Alloys Compd. **488**, 129-133 (2010).
[58] U. Sarı, T. Kırındı, Materials Chemistry and Physics **130**, 738-742 (2011).
[59] Y.U.L. Rodionov, G.G. Isfandiyarov, V.N. Zambrzhitskiy, Phys. Met. Metall. **49**, 94-100 (1980).
[60] P. Panissod, J Durand, J.I. Budnick, Nucl. Instrum. Methods **199**, 99-114 (1982).
[61] K. Yamauchi, T. Mızoguchi, J. Phys. Soc. Jpn. **39**, 541-542 (1975).
[62] D. Bandyopadhyay, S. Suwas, R.M. Singru, S. Bhargava, J. Mater. Sci. **33**, 109 (1998).
[63] Z. Qin, Y. Zhang, Hyperfine Int. **116**, 225 (1998).
[64] A.S.M.A. Haseeb, T. Nishida, M. Masuda, Y. Hayashi, Scripta. Mater. **44**, 519 (2001).
[65] X. Lu, B. Zhang, Z. Qin, Y. Zhang, B. Ding, Z. Hu, Mater. Sci. Eng. A **347**, 258-264 (2003).
[66] J. Jung, M. Fricke, G. Hampel, J. Hesse, Hyp. Interact. **72**, 375 (1992).
[67] M. Nabialek, Revista de Chimie **69**, 4, 802-805, (2018).
[68] J. Olszewski, J. Zbroszczyk, K. Sobczyk, W. Ciurzynska, P. Bragiel, M. Nabialek, J. Swierczek, M. Hasiak, A. Lukiewska, Acta Physica Polonica A **114**, 6, 1659-1666, (2008).
[69] M. Nabialek, J. Zbroszczyk, J. Olszewski, M. Hasiak, W. Ciurzynska, K. Sobczyk, J. Swierczek, J. Kaleta, A. Lukiewska, Journal of Magnetism and Magnetic Materials **320**, 787-791, (2008).